



Deposited via The University of Sheffield.

White Rose Research Online URL for this paper:

<https://eprints.whiterose.ac.uk/id/eprint/191773/>

Version: Accepted Version

Article:

Lyons, T.P., Gillard, D.J., Leblanc, C. et al. (2022) Giant effective Zeeman splitting in a monolayer semiconductor realized by spin-selective strong light–matter coupling. *Nature Photonics*, 16 (9). pp. 632-636. ISSN: 1749-4885

<https://doi.org/10.1038/s41566-022-01025-8>

This is a post-peer-review, pre-copyedit version of an article published in *Nature Photonics*. The final authenticated version is available online at:
<http://dx.doi.org/10.1038/s41566-022-01025-8>.

Reuse

Items deposited in White Rose Research Online are protected by copyright, with all rights reserved unless indicated otherwise. They may be downloaded and/or printed for private study, or other acts as permitted by national copyright laws. The publisher or other rights holders may allow further reproduction and re-use of the full text version. This is indicated by the licence information on the White Rose Research Online record for the item.

Takedown

If you consider content in White Rose Research Online to be in breach of UK law, please notify us by emailing eprints@whiterose.ac.uk including the URL of the record and the reason for the withdrawal request.

Giant effective Zeeman splitting in a monolayer semiconductor realized by spin-selective strong light-matter coupling

T. P. Lyons,^{1,2,3,*} D. J. Gillard,^{1,3} C. Leblanc,^{4,3} J. Puebla,⁵ D. D. Solnyshkov,^{4,6} L. Klompmaker,⁷ I. A. Akimov,^{7,8} C. Louca,¹ P. Muduli,^{9,10} A. Genco,¹ M. Bayer,^{7,8} Y. Otani,^{5,11} G. Malpuech,⁴ and A. I. Tartakovskii^{1,†}

¹*Department of Physics and Astronomy, The University of Sheffield, Sheffield S3 7RH, UK*

²*Present address: RIKEN Center for Emergent Matter Science, Wako, Saitama 351-0198, Japan*

³*These authors contributed equally to this work*

⁴*Institut Pascal, PHOTON-N2, CNRS, Université Clermont Auvergne, F63000 Clermont-Ferrand, France*

⁵*RIKEN Center for Emergent Matter Science, Wako, Saitama 351-0198, Japan*

⁶*Institut Universitaire de France (IUF), F-75231 Paris, France*

⁷*Experimentelle Physik 2, Technische Universität Dortmund, 44221 Dortmund, Germany*

⁸*Ioffe Institute, Russian Academy of Sciences, 194021 St. Petersburg, Russia*

⁹*Institute for Solid State Physics, University of Tokyo, Kashiwa 277-8581, Japan*

¹⁰*Present address: Department of Physics, Indian Institute of Technology Madras, Chennai 600036, India*

¹¹*Institute for Solid State Physics, University of Tokyo, Kashiwa, Chiba 277-8581, Japan*

(Dated: May 10, 2022)

Strong coupling between light and the fundamental excitations of a two-dimensional electron gas (2DEG) are of foundational importance both to pure physics and to the understanding and development of future photonic nanotechnologies [1–7]. Here we study the relationship between spin polarization of a 2DEG in a monolayer semiconductor, MoSe₂, and light-matter interactions modified by a zero-dimensional optical microcavity. We find pronounced spin-susceptibility of the 2DEG to simultaneously enhance and suppress trion-polariton formation in opposite photon helicities. This leads to observation of a giant effective valley Zeeman splitting for trion-polaritons (g-factor > 20), exceeding the purely trionic splitting by over five times. Going further, we observe clear effective optical non-linearity arising from the highly non-linear behavior of the valley-specific strong light-matter coupling regime, and allowing all-optical tuning of the polaritonic Zeeman splitting from 4 to > 10 meV. Our experiments lay the groundwork for engineering topological phases with true unidirectionality in monolayer semiconductors, accompanied by giant effective photonic nonlinearities rooted in many-body exciton-electron correlations.

MAIN

Monolayer MoSe₂ presents a four-band massive Dirac system for studying spin and valley pseudospin dependent interactions between electrons, excitons, and photons [3, 4]. In the presence of an appreciable free carrier density, simple neutral exciton absorption evolves into two Fermi-polaron branches, repulsive and attractive [2–4, 7]. The monolayer then plays host to a Bose-Fermi mixture consisting of excitons dressed by electrons (or holes, for *p*-type doping). Strong coupling of these Fermi-polaron resonances to photonic microcavity modes has been demonstrated [4, 5]. Simplistically, the repulsive and attractive polarons correspond to a spin-triplet or spin-singlet interaction, respectively, between the two-dimensional electron gas (2DEG) and the constituent electron of the exciton [3, 4, 7]. In MoSe₂, subject to strict spin-valley locking and chiral optical selection rules, this has the consequence of tying the 2DEG degree of spin polarization to the oscillator strengths of the polaron resonances in opposite photon helicities. The extreme example of this effect is when the 2DEG becomes fully spin polarized, leading to vanishing absorption of the attractive polaron in one photon helicity [3, 7].

It has recently been reported that when the Fermi level is significantly smaller than the trion binding energy,

the attractive polaron may be adequately described as a three-body charged exciton, or trion [8, 9]. Although nominally the trion exists only in the strict single particle limit, in reality the transition between these two quasi-particle regimes is unclear, and likely depends heavily on the degree of exciton and carrier spatial localization over the monolayer, especially at low densities. This is particularly true in the case of nonequilibrium scenarios such as photoluminescence experiments, in which both species may coexist [9].

Valley Zeeman splitting of these excitonic complexes has been reported under application of strong out-of-plane magnetic fields (B-fields) [3, 6, 10]. However, translating the relatively large Zeeman splitting of a purely matter-bound excitation into a photonic mode splitting remains a fundamental challenge not only in opto-valleytronics [11], but also in topological photonics. Indeed, many topological states of light have been implemented in recent years [12], including using TMD exciton-polaritons [13, 14]. The ultimate goal of real topological protection against any type of disorder scattering and back-reflection requires time-reversal symmetry breaking [15, 16], with the size of the topological gap limited by the effective Zeeman splitting of the photonic modes. Large splittings are difficult to achieve at optical frequencies, and in the existing realizations either

based on the use of magnetic proximity effects [17] or on the matter-based Zeeman splitting of exciton-polaritons [18, 19], the topological gap was < 1 meV, too small to be clearly observable.

In our work, by harnessing many-body interactions in a 2-dimensional Bose-Fermi mixture, we realize a giant effective trion-polariton Zeeman splitting, over 5 times larger than the bare (uncoupled) trion splitting, and more than double the polariton linewidths, a crucial step towards elimination of unwanted coupling between chiral modes [20]. We moreover demonstrate giant effective non-linearity $\alpha \approx 0.2 \pm 0.05$ meV $\cdot\mu\text{m}^2$ for trion-polaritons under a magnetic field. This value is one order of magnitude larger than previously reported in TMDs [5, 21] and is based on an original mechanism involving free carrier valley relaxation and strong light-matter coupling. Large photonic non-linearities, as in this work, are crucial for classical, quantum and topological photonics [12, 16].

We study a MoSe₂ monolayer on a 10 nm thick film of the ferromagnetic semiconductor europium sulfide (EuS) which coats a dielectric distributed Bragg reflector (DBR). Firstly, we characterize the MoSe₂ monolayer in the half-cavity, or bare flake, configuration, at temperature $T = 4.2$ K. Fig. 1a shows circular polarization resolved reflectance contrast ($\text{RC} = (R_0 - R)/R_0$, where R and R_0 are the reflectance from the MoSe₂ and adjacent EuS substrate, respectively) spectra from the sample under linearly polarized broadband illumination at out-of-plane magnetic field strengths $B = -8, 0, +8$ T. We observe, at $B = 0$ T, two clear absorption peaks attributed to the neutral exciton (X_{RC}) and trion (T_{RC}) at higher and lower energy, respectively. T_{RC} displays a significant spectral weight, indicating an elevated doping level of the flake. These two resonances may be similarly described as Fermi-polarons, sharing the fundamental principle of a neutral exciton being either bound (attractive interaction, trion-like) or unbound (repulsive interaction) to itinerant carriers [2–4, 7]. The energy separation between these peaks allows us to estimate the free carrier density as 10^{12} cm⁻² (see Supplementary Note 1) [7]. We attribute this relatively high carrier density to electron doping from the EuS film, which we expect to be highly charged owing to the deposition technique (see Methods) [22, 23]. Measuring photoluminescence (PL) using a continuous wave laser at 1.946 eV, only a single peak is observed, attributed to the trion. The absence of neutral exciton PL is consistent with the high doping level in the flake, as is the significant Stokes shift of ~ 6 meV observed between T_{RC} and T_{PL} (Fig. 1a) [4].

When $B = \pm 8$ T, T_{RC} is only visible in one circular polarization (Fig. 1a). Owing to its spin-singlet or inter-valley nature, the trion absorption strength of σ^+ (σ^-) light depends upon the itinerant carrier density in the $-K$ ($+K$) valley. Therefore, the electron Zeeman splitting is sufficiently large at this temperature to fully spin polarize the 2DEG (Fig. 1b) (see Supplementary Note 2)

[3, 7]. Achieving complete spin polarization of a 2DEG of such high density as here may point to itinerant ferromagnetism, in which transient domains of oppositely spin polarized electrons at $B = 0$ T evolve into a spatially correlated spin polarized state when $B > 0$ T [24, 25]. We additionally note that while EuS is ferromagnetic, we see no evidence of magnetic proximity effects in the sample (see Supplementary Note 3).

For the next stage of the study, we incorporate the MoSe₂ / EuS structure into a tunable zero-dimensional microcavity (Fig. 1c), formed by introducing a downward facing top concave DBR into the optical path above the sample (as described in Ref. [26]). By control of the mirror separation using piezo nanopositioners, we tune the ground state longitudinal cavity mode (Laguerre-Gaussian LG_{00}) through resonance with both T_{PL} and T_{RC} , and perform cavity PL spectroscopy using a linearly polarized laser at power $5\mu\text{W}$. At $B = 0$ T, we observe essentially identical PL spectra for both σ^+ and σ^- detection polarizations. As the cavity length is tuned, the observation of an anticrossing indicates strong light-matter coupling and defines upper and lower trion-polariton branches (UPB and LPB) separated by a Rabi splitting $\Omega_R \sim 9$ meV. We note here that the trion Stokes shift is comparable with the Rabi splitting, and therefore must be taken into account in order to precisely fit the polariton PL energies by going beyond the most basic coupled oscillator model (see Supplementary Note 2). Indeed, while the anticrossing originates at the energy of T_{RC} , where cavity photons are most strongly absorbed, the polariton PL shows a finite Stokes shift causing both UPB and LPB emission to tend to the trion PL energy at vanishing photon fractions. Repeating the experiment at $B = +8$ T (Fig. 1d) reveals a larger anticrossing in σ^+ , while the strong coupling regime breaks down in σ^- (Ω_R is smaller than the polariton linewidths and unresolved), consistent with the weak oscillator strength of T_{RC} in σ^- (Fig. 1a top panel), and constituting observation of valley-specific strong light-matter coupling, in which trions of opposite valley pseudospin are respectively strongly coupled to σ^+ light while only weakly coupled to σ^- light.

Fig. 2a shows polarization resolved LPB PL versus piezo voltage at $B = 0$ and $+8$ T, revealing a giant effective Zeeman splitting exceeding 10 meV, whereby the large anticrossing displayed by $+K$ valley trion-polaritons, absent for the $-K$ valley, gives rise to a clear energy separation between σ^+ and σ^- polarized modes. This occurs because the near-unity spin polarization of the 2DEG at $B = +8$ T suppresses the oscillator strength of the trion in σ^- polarization, by transferring it to σ^+ polarization. Fig. 2b compares the trion PL g-factor measured on the bare flake ($g = 3.9$) with that of the trion-polariton which is over 5 times larger ($g = 21.1$). While the LPB Zeeman splitting increases at higher voltages, this comes at the cost of increased polari-

180 ton linewidths and reduced intensity. However, we note
 181 that the LPB Zeeman splitting exceeds the bare trion
 182 splitting for all B-field strengths and all cavity lengths
 183 studied here. This result is in marked contrast to the
 184 expected scenario in which the polariton valley Zeeman
 185 splitting is reduced relative to that of bare trion by the
 186 corresponding Hopfield coefficient [27].

187 Next, we show how the giant Zeeman splitting can be
 188 very effectively optically controlled. We fix $B = +8$ T
 189 and study the influence of incident laser power on the
 190 cavity PL. As can be seen in Fig. 3a, increased power re-
 191 opens the anticrossing in σ^- which previously collapsed
 192 upon application of the B-field (Fig. 1d). Fig. 3b shows
 193 trion-polariton PL spectra versus pumping power at fixed
 194 cavity length, where Ω_R grows in σ^- and correspondingly
 195 decays in σ^+ , suggesting that non-resonant pumping effi-
 196 ciently transfers electrons between spin states (equiva-
 197 lently, between valley states, see Fig. 1b). Here, quali-
 198 tatively, electron-hole pairs are injected by the laser and
 199 bind to form excitons and trions on ultrafast timescales
 200 (sub-ps). The initial trion population will be highly val-
 201 ley polarized as the only free carriers available are from
 202 the spin polarized 2DEG, however, exciton and trion val-
 203 ley depolarization in MoSe₂ is extremely efficient (ps)
 204 owing to the Maialle-Silva-Sham (MSS) mechanism (con-
 205 firmed here by transient ellipticity measurements, see
 206 Supplementary Note 4) [26, 28]. Therefore, rapid in-
 207 tervalley scattering of trions followed by their radiative
 208 decay can result in a free electron remaining in the spin
 209 state anti-aligned to the external B-field. This means
 210 that each trion emission process results in partial trans-
 211 fer of electrons between spin-valley states. While trion
 212 valley relaxation occurs on ps timescales, the spin relax-
 213 ation time for free electrons is ~ 1000 times longer, of
 214 the order ns, as they are immune to the MSS mecha-
 215 nism and must undergo a large momentum transfer to
 216 scatter between spin-valley states. As such, trion in-
 217 tervalley scattering and subsequent photon emission can
 218 depolarize the 2DEG ~ 1000 times faster than it can re-
 219 turn to spin-polarized equilibrium. By embedding all of
 220 these processes into rate equations, we infer that laser
 221 power in the μ W range is enough to fully balance the
 222 2DEG spin populations and associated trion-polariton
 223 Rabi splittings in opposite circular polarizations. Our
 224 simulations are shown in Fig. 3c (top panel) and are in
 225 excellent agreement with experimental data.

226 Lastly, we relate the computed exciton and trion densi-
 227 ties to the energy shifts of the LPB when $B = +8$ T, and
 228 deduce effective LPB interaction strengths, in this case
 229 attractive for σ^- and repulsive for σ^+ . The middle panel
 230 of Fig. 3c shows the LPB blueshift in σ^+ alongside the effe-
 231 ctive interaction strength, defined as $\alpha = \partial E_{LPB}^+ / \partial n^+$
 232 (see Supplementary Note 2), which corresponds to a
 233 repulsive interaction between same-spin particles since
 234 only σ^+ excitons can depolarize electrons when $B = +8$
 235 T. The extracted value, $\alpha \approx 0.2 \pm 0.05$ meV $\cdot\mu\text{m}^2$ at

236 $P = 5$ μ W, is one order of magnitude larger than pre-
 237 viously reported for trion-polaritons because it is based
 238 on a completely different mechanism [21]. It is based
 239 neither on oscillator strength or the Coulomb interaction
 240 between carriers, but instead on linear spin relaxation
 241 processes. The increase in the interaction strength at the
 242 lowest laser powers is accompanied by a marked increase
 243 in the effective trion-polariton Zeeman splitting, confirm-
 244 ing their shared origin in the 2DEG spin dynamics (Fig.
 245 3c bottom panel).

246 Our experiments demonstrate the simultaneous mani-
 247 festation of strong and weak coupling regimes between a
 248 photonic mode and a many-body correlated matter exci-
 249 tation consisting of an exciton dressed by electrons in an
 250 effective ferromagnetic phase, resulting in a giant Zeeman
 251 splitting between trion-polariton modes. We addition-
 252 ally show that laser illumination acts to depolarize the
 253 2DEG via a process of trion valley pseudospin relaxation
 254 and subsequent radiative recombination. The resulting
 255 Rabi splitting transfer between the two polarization com-
 256 ponents induces energy renormalization to which we as-
 257 sociate large effective interactions. While in this work
 258 an EuS film was used to introduce additional free elec-
 259 trons into the flake, similar results should be observed
 260 in any MoSe₂ monolayer in which the itinerant carrier
 261 density can be raised arbitrarily to give the trion suffi-
 262 cient oscillator strength. Magnetic 2-dimensional ma-
 263 terials may also be used to induce 2DEG spin polariza-
 264 tion without the need for strong external B-fields [25].
 265 Moreover, we note that extremely high laser powers, of-
 266 ten pulsed and quasi-resonant, are typically needed to
 267 enter regimes of polariton non-linearity, while here the
 268 strongest effective interactions occur under low power
 269 non-resonant continuous-wave laser excitation. Our work
 270 therefore highlights doped MoSe₂ as a flexible system in
 271 which to realize and apply ultrastrong low-threshold non-
 272 linearities, for instance towards TMD-based all-optical
 273 logic gates [29], or to explore nonlinear topological pho-
 274 tonics [30].

275 ACKNOWLEDGEMENTS

276 TPL acknowledges financial support from the EPSRC
 277 Doctoral Prize Fellowship scheme under Grant Refer-
 278 ence EP/R513313/1, and the JSPS Postdoctoral Fellow-
 279 ships for Research in Japan scheme. TPL, DJG, JP, YO
 280 and AIT acknowledge support from the Royal Society
 281 International Exchange Grant IEC\R3\170088. TPL,
 282 DJG, AG, CLo, LK, IA, MB and AIT acknowledge EP-
 283 SRC Centre-to-Centre grant EP/S030751/1. TPL, DJG
 284 and AIT additionally acknowledge financial support of
 285 the European Graphene Flagship Project under grant
 286 agreement 881603 and EPSRC grants EP/V006975/1,
 287 EP/P026850/1 and EP/V026496/1. CLe, DS and GM
 288 acknowledge the support of the projects EU “TOPO-

289 LIGHT” (964770), “QUANTOPOL” (846353), of the
 290 ANR Labex GaNEXT (ANR-11-LABX-0014), and of
 291 the ANR program “Investissements d’Avenir” through
 292 the IDEX-ISITE initiative 16-IDEX-0001 (CAP 20-25).
 293 LK, IA and MB acknowledge financial support by the
 294 Deutsche Forschungsgemeinschaft through the Interna-
 295 tional Collaborative Research Centre 160 (Project No.
 296 C2) and UAR professorship: Mercur Foundation (grant
 297 Pe-2019-0022). The authors thank D. N. Krizhanovskii
 298 for useful discussions.

AUTHOR CONTRIBUTIONS

300 TPL, DJG and JP performed low temperature
 301 magneto-optical spectroscopy. TPL, DJG, CLe, DDS,
 302 GM and AIT analyzed and discussed the bare flake and
 303 cavity spectroscopy data. CLe, DDS and GM developed
 304 the cavity fitting model and rate equations. LK and
 305 IAA collected and analyzed time-resolved data. JP and
 306 PM deposited the EuS films onto DBR substrates. TPL,
 307 DJG, JP and PM performed SQUID magnetometry. CLo
 308 identified and transferred MoSe₂ flakes onto EuS films.
 309 AG carried out electron density calculations. MB, YO,
 310 GM and AIT managed various aspects of the project.
 311 AIT supervised the project. TPL wrote the manuscript
 312 with contributions from all co-authors.

COMPETING INTERESTS

314 The authors declare no competing interests.

FIGURE CAPTIONS

REFERENCES

- 317 * thomas.lyons@riken.jp
 318 † a.tartakovskii@sheffield.ac.uk
- 319 [1] Smolka, S. *et al.* Cavity quantum electrodynamics with
 320 many-body states of a two-dimensional electron gas. *Sci-*
 321 *ence* **346**, 332–335 (2014).
 322 [2] Efimkin, D. K. & MacDonald, A. H. Many-body theory
 323 of trion absorption features in two-dimensional semicon-
 324 ductors. *Physical Review B* **95**, 035417 (2017).
 325 [3] Back, P. *et al.* Giant paramagnetism-induced valley
 326 polarization of electrons in charge-tunable monolayer
 327 MoSe₂. *Physical Review Letters* **118**, 237404 (2017).
 328 [4] Sidler, M. *et al.* Fermi polaron-polaritons in charge-
 329 tunable atomically thin semiconductors. *Nature Physics*
 330 **13**, 255–261 (2017).
 331 [5] Tan, L. B. *et al.* Interacting polaron-polaritons. *Physical*
 332 *Review X* **10**, 021011 (2020).
 333 [6] Klein, J. *et al.* Controlling exciton many-body states
 334 by the electric-field effect in monolayer MoS₂. *Physical*
 335 *Review Research* **3**, L022009 (2021).
 336 [7] Roch, J. G. *et al.* Spin-polarized electrons in monolayer
 337 MoS₂. *Nature Nanotechnology* **14**, 432–436 (2019).
 338 [8] Glazov, M. M. Optical properties of charged excitons
 339 in two-dimensional semiconductors. *Journal of Chemical*
 340 *Physics* **153**, 034703 (2020).
 341 [9] Imamoglu, A., Cotlet, O. & Schmidt, R. Exciton-
 342 polarons in two-dimensional semiconductors and the
 343 Tavis-Cummings model. *Comptes Rendus. Physique* **22**,
 344 S4, 89–96 (2021).
 345 [10] MacNeill, D. *et al.* Breaking of valley degeneracy by mag-
 346 netic field in monolayer MoSe₂. *Physical Review Letters*
 347 **114**, 037401 (2015).
 348 [11] Langer, F. *et al.* Lightwave valleytronics in a monolayer
 349 of tungsten diselenide. *Nature* **557**, 76–80 (2018).
 350 [12] Ozawa, T. *et al.* Topological photonics. *Reviews of Mod-*
 351 *ern Physics* **91**, 015006 (2019).
 352 [13] Li, M. *et al.* Experimental observation of topological
 353 Z₂ exciton-polaritons in transition metal dichalcogenide
 354 monolayers. *Nature Communications* **12**, 4425 (2021).
 355 [14] Liu, W. *et al.* Generation of helical topological exciton-
 356 polaritons. *Science* **370**, 600–604 (2020).
 357 [15] Wang, Z., Chong, Y., Joannopoulos, J. D. & Soljačić,
 358 M. Observation of unidirectional backscattering-immune
 359 topological electromagnetic states. *Nature* **461**, 772–775
 360 (2009).
 361 [16] Lu, L., Joannopoulos, J. D. & Soljačić, M. Topological
 362 photonics. *Nature Photonics* **8**, 821–829 (2014).
 363 [17] Bahari, B. *et al.* Nonreciprocal lasing in topological cav-
 364 ities of arbitrary geometries. *Science* **358**, 636–640 (2017).
 365 [18] Nalitov, A. V., Solnyshkov, D. D. & Malpuech, G. Pol-
 366 ariton Z topological insulator. *Physical Review Letters*
 367 **114**, 116401 (2015).
 368 [19] Klembt, S. *et al.* Exciton-polariton topological insulator.
 369 *Nature* **562**, 552–556 (2018).
 370 [20] Song, W. *et al.* Breakup and recovery of topological zero
 371 modes in finite non-Hermitian optical lattices. *Physical*
 372 *Review Letters* **123**, 165701 (2019).
 373 [21] Emmanuele, R. P. A. *et al.* Highly nonlinear trion-
 374 polaritons in a monolayer semiconductor. *Nature Com-*
 375 *munications* **11**, 3589 (2020).
 376 [22] Keller, J. *et al.* Controlling the magneto-transport prop-
 377 erties of EuS thin films. *IEEE Transactions on Magnetics*
 378 **38**, 2673–2675 (2002).
 379 [23] Grzeszczyk, M. *et al.* The effect of metallic substrates
 380 on the optical properties of monolayer MoSe₂. *Scientific*
 381 *Reports* **10**, 4981 (2020).
 382 [24] Roch, J. G. *et al.* First-order magnetic phase transition
 383 of mobile electrons in monolayer MoS₂. *Physical Review*
 384 *Letters* **124**, 187602 (2020).
 385 [25] Lyons, T. P. *et al.* Interplay between spin proximity ef-
 386 fect and charge-dependent exciton dynamics in MoSe₂ /
 387 CrBr₃ van der Waals heterostructures. *Nature Commu-*
 388 *nications* **11**, 6021 (2020).
 389 [26] Dufferwiel, S. *et al.* Valley-addressable polaritons in
 390 atomically thin semiconductors. *Nature Photonics* **11**,
 391 497–501 (2017).
 392 [27] Lundt, N. *et al.* Magnetic-field-induced splitting and pol-
 393 arization of monolayer-based valley exciton polaritons.
 394 *Physical Review B* **100**, 121303(R) (2019).
 395 [28] Glazov, M. M. *et al.* Exciton fine structure and spin
 396 decoherence in monolayers of transition metal dichalco-

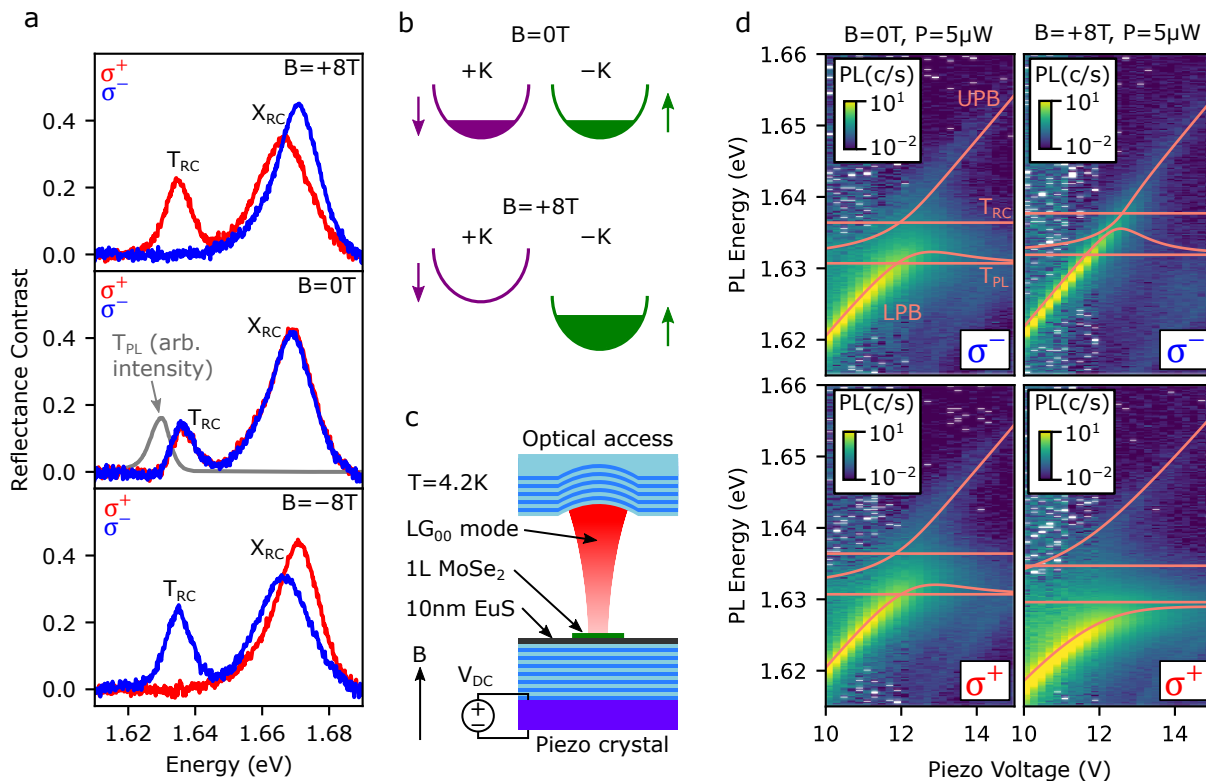


FIG. 1. **Excitations of a 2-dimensional electron gas strongly coupled to light in monolayer MoSe₂.** (a) Reflectance contrast $RC = (R_0 - R)/R_0$ from monolayer MoSe₂ (reflectance R on flake and R_0 on substrate) with raised itinerant carrier density at $T = 4.2$ K and $B = -8, 0, +8$ T. Two peaks are attributed to the neutral exciton (X_{RC}) and charged exciton or trion (T_{RC}). At high B-fields the trion absorption is completely suppressed in one or the other circular polarization of light. For comparison the trion photoluminescence T_{PL} signal at $B = 0$ T is also shown, revealing a Stokes shift of ~ 6 meV. Neutral exciton emission is absent owing to the raised doping level of the flake and rapid trion formation. (b) Sketch of the lowest conduction sub-bands of monolayer MoSe₂, in which the electronic spin and valley pseudospin ($+K$ or $-K$ valley of momentum space) are strictly correlated. These degrees of freedom are distinct in that the spin couples to magnetic field, while the valley pseudospin couples to light. Optical selection rules dictate that excitons and trions of $+K$ ($-K$) valley pseudospin couple, weakly or strongly, to σ^+ (σ^-) polarized photons. At $B = 0$ T, the 2DEG has zero net spin polarization. At $B = +8$ T, the 2DEG is completely spin polarized, causing the oscillator strength of the $-K$ valley trion to be suppressed owing to a lack of itinerant electrons in the $+K$ valley. (c) Schematic of the zero-dimensional open cavity structure used in this work. Applying a DC voltage to the piezo crystal decreases the cavity length (see Methods). (d) Cavity PL intensity maps (counts/s, logarithmic scale) as the cavity mode is tuned through the trion resonances. Shown are the results at $B = 0$ T (left panels) and $B = +8$ T (right panels) in both photon emission helicities. The laser is linearly polarized. At $B = 0$ T, the spectra are essentially identical between both polarizations, while the near-unity spin polarization of the 2DEG at $B = +8$ T causes strong coupling to break down in σ^- polarization. A modified coupled oscillator model incorporating the trion-polariton Stokes shift was used to fit the UPB and LPB (overlaid orange curves). The energies of T_{PL} and T_{RC} in both polarizations (orange horizontal lines) are obtained directly or inferred from bare flake spectra at $B = 0$ T and $+8$ T. The UPB becomes progressively dimmer at higher energies owing to increasing absorption from the EuS film.

- 397 genides. *Physical Review B* **89**, 201302(R) (2014). 403
 398 [29] Amo, A. *et al.* Exciton-polariton spin switches. *Nature*
 399 *Photonics* **4**, 361–366 (2010).
 400 [30] Smirnova, D., Leykam, D., Chong, Y. & Kivshar, Y. 404
 401 Nonlinear topological photonics. *Applied Physics Reviews*
 402 **7**, 021306 (2020).

METHODS

Low temperature magneto-optical spectroscopy

405 Magneto-optical spectroscopy at 4.2 K was performed
 406 by mounting the sample in a liquid helium bath cryostat
 407 with a superconducting magnet and free space optical ac-
 408 cess. Reflectance contrast measurements were performed
 409 by directing broadband white light in either σ^+ or σ^- cir-
 410 cular polarization onto the sample and measuring the re-

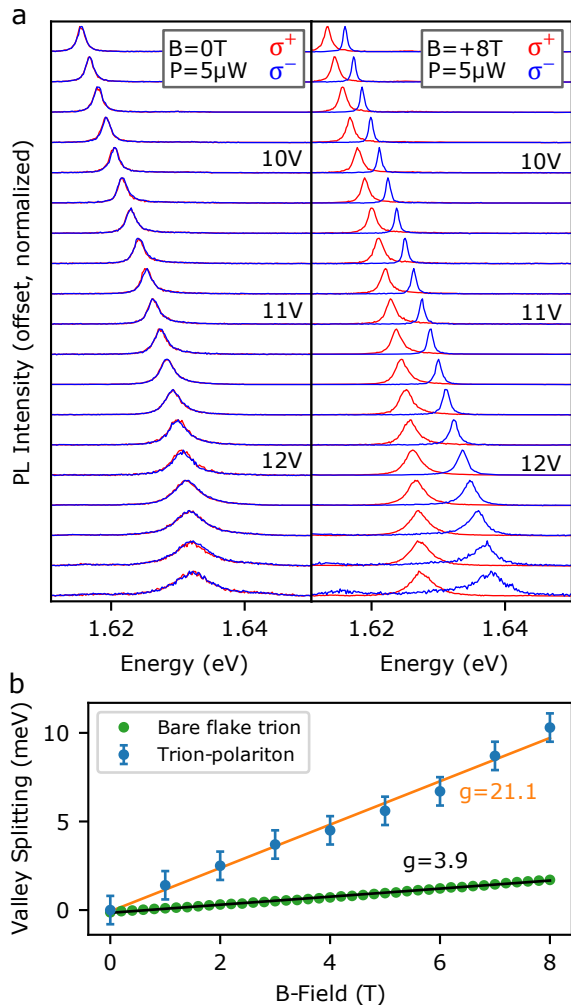


FIG. 2. **Giant effective trion-polariton Zeeman splitting.** (a) Cavity PL spectra at increasing piezo voltages (decreasing cavity length) for $B = 0\text{ T}$ (left panel) and $B = +8\text{ T}$ (right panel). A giant Zeeman splitting of the lower polariton branch (LPB) can be seen when the B-field is applied. Spectra normalization factors at $B = +8\text{ T}$ are stable around ~ 1.2 from 9.2 V to 11.6 V, increasing to 6.6 at 12.8 V owing to onset of absorption from the EuS film, which reduces the cavity Q-factor and weakens σ^- intensity. (b) The maximum valley splitting of the trion-polariton LPB as a function of applied B-field strength. Here, we extract an effective maximum LPB Zeeman splitting at each 1 T B-field increment from our cavity fitting procedure (see Supplementary Note 2). Error bars quantify the uncertainty arising from fitting the spectral PL peaks to Lorentzian functions to extract peak energies. For comparison the valley Zeeman splitting of the bare (uncoupled) trion is also shown. The g-factors of the trion-polariton and bare trion are (21.1 ± 0.9) and (3.93 ± 0.04) , respectively.

413 Photoluminescence spectroscopy was performed by di-
 414 recting a linearly polarized continuous wave laser at 1.946
 415 eV onto the sample and detecting the emission in either
 416 σ^+ or σ^- circular polarization. For both RC and PL the
 417 signal was directed through a single mode fiber to a 0.75
 418 m spectrometer and onto a nitrogen-cooled high sensitiv-
 419 ity charge-coupled device (see Supplementary Note 5).

420 The tunable zero-dimensional open microcavity is
 421 formed by bringing a concave top DBR into the opti-
 422 cal path above the planar bottom DBR, on top of which
 423 is the 10 nm EuS film and monolayer MoSe₂. The EuS
 424 film serves to increase the itinerant electron density in
 425 the MoSe₂. A gap filled with helium exchange gas sep-
 426 arates the DBRs forming a zero-dimensional optical mi-
 427 crocavity. Piezo nanopositioners allow precise tuning of
 428 the cavity length, whereby applying a DC voltage will
 429 decrease the cavity length and increase the energy of the
 430 ground state zero-dimensional Laguerre-Gaussian mode
 431 (LG_{00}) such that it can be tuned through resonance with
 432 both T_{PL} and T_{RC} .

433 Europium sulfide deposition

434 A 10 nm thick film of europium sulfide (EuS) was
 435 deposited onto a dielectric DBR (top layer SiO₂) by
 436 electron-beam evaporation. By maintaining a low sub-
 437 strate temperature of 16 °C during the deposition, we
 438 ensure that the resulting EuS film will be sulfur deficient,
 439 owing to the much lower vapor pressure of S relative to
 440 Eu, causing S atoms to re-evaporate from the substrate
 441 during growth. The resulting sulfur vacancies act as elec-
 442 tron donors causing the non-stoichiometric EuS film to
 443 act as a heavily-doped ferromagnetic semiconductor [22].
 444 The MoSe₂ monolayer therefore becomes highly charged
 445 when it is stamped on top of the EuS substrate [23].

446 Sample fabrication

447 A MoSe₂ bulk crystal supplied by HQ Graphene
 448 was exfoliated with tape onto a polydimethylsiloxane
 449 (PDMS) sheet, and a suitable monolayer identified by
 450 optical microscopy. This monolayer was then stamped
 451 onto the DBR / EuS substrate using a conventional vis-
 452 coelastic dry transfer method.

453 Data Availability

454 Data supporting the plots within this paper is available
 455 from the corresponding authors upon request.

411 flected signal on the MoSe₂ monolayer (R) and adjacent
 412 bare EuS film (R_0), and calculating the $RC = \Delta R/R$.

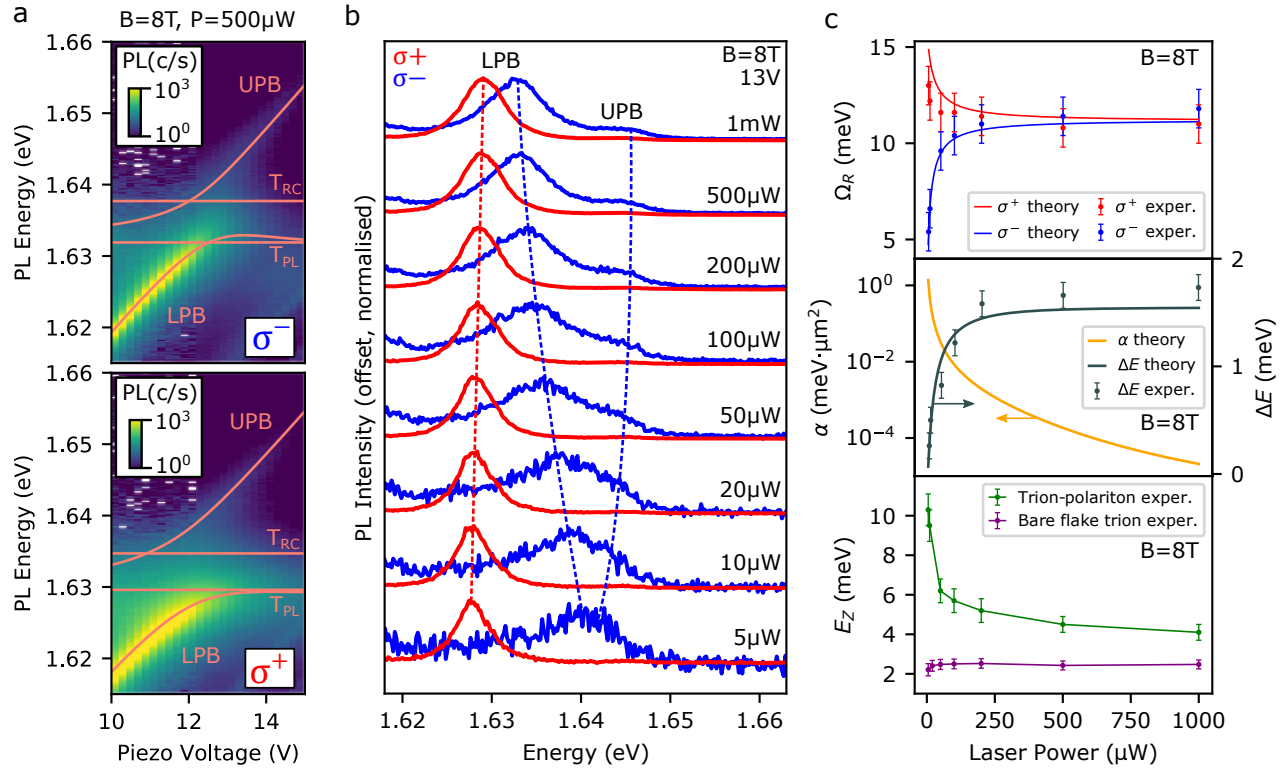


FIG. 3. Trion-polariton effective nonlinearity. (a) Cavity PL intensity colormaps (counts/s, logarithmic scale) in σ^+ and σ^- emission at $B = +8\text{ T}$ and a high laser power $P = 500\ \mu\text{W}$. An anticrossing is seen in both polarizations despite the strong applied B-field. Polariton fitting curves incorporating the Stokes shift are overlaid. (b) Cavity PL spectra at fixed detuning close to trion-cavity resonance, at $B = +8\text{ T}$, taken at varying incident laser powers. As the power is decreased, the 2DEG spin polarization increases and the anticrossing in σ^- is suppressed. This has the secondary effect of amplifying the effective Zeeman splitting between σ^+ and σ^- lower polaritons. (c) (top panel) Rabi splittings, Ω_R , in σ^+ and σ^- at $B = +8\text{ T}$ against laser power. Nonlinear breakdown of strong coupling in σ^- is observed as the power is decreased. Solid curves are simulated results (see Supplementary Note 2). (middle panel) The calculated effective trion-polariton interaction strength, α (see main text for definition), and the calculated and experimental blueshift, ΔE , of the LPB in σ^+ polarization, both at $B = +8\text{ T}$ as a function of pump power. As there is no emission at $0\ \mu\text{W}$, the blueshift between 0 and $5\ \mu\text{W}$ is assumed to be the same as between 5 and $10\ \mu\text{W}$, measured as $(0.23 \pm 0.12)\text{ meV}$. (lower panel) The maximum LPB Zeeman splitting, E_Z , at $B = +8\text{ T}$ against laser power. The splitting increases drastically at the lowest powers when the 2DEG spin polarization is highest. For comparison the bare trion Zeeman splitting is shown. Error bars on experimental data points quantify the uncertainty arising from fitting spectral PL peaks to Lorentzian functions to extract peak energies.